This is a repository copy of *Encapsulation of emulsion droplets with metal shells for subsequent remote, triggered release.*.

White Rose Research Online URL for this paper:
http://eprints.whiterose.ac.uk/143911/

Version: Accepted Version

Encapsulation of emulsion droplets with metal shells for subsequent remote, triggered release

Kirsty Stark[1], James P. Hitchcock[1], Assim Fiaz[1], Alison L. White[2], Elaine A. Baxter[3], Simon Biggs[4], James R. McLaughlan[5,6], Steven Freear[5] and Olivier J. Cayre[1]

1. School of Chemical and Process Engineering, University of Leeds, LS2 9JT, UK

2. Australian Institute for Bioengineering and Nanotechnology, University of Queensland, St Lucia 4072, Queensland, Australia

3. Procter & Gamble, Greater London Innovation Centre, Egham, Surrey, TW20 9NW, UK

4. The University of Western Australia, Perth WA, 6009, Australia

5. School of Electronic and Electrical Engineering, University of Leeds, LS2 9JT, UK

6. Leeds Institute of Medical Research, University of Leeds, St. James's University Hospital, LS9 7TF

ABSTRACT: A 2-step method to encapsulate an oil core with an impermeable shell has been developed. A thin metallic shell is deposited on the surface of emulsion droplets stabilised by metal nanoparticles. This thin shell is shown to prevent diffusion of the oil from within the core of the metal-shell microcapsules when placed in a continuous phase that fully dissolves the oil. The stabilising nanoparticles are sterically-stabilised by poly(vinyl pyrrolidone) chains and are here used as a catalyst/nucleation site at the oil-water interface to grow a secondary metal shell on the emulsion droplets via an electroless deposition process. This method provides the simplest scalable route yet to synthesise impermeable microcapsules with the added benefit that the final structure allows for drastically improving the overall volume of encapsulated core to, in this case, >99% of the total volume. This method also allows for very good control over the microcapsule properties and here we demonstrate our ability to tailor the final microcapsule density, capsule diameter and secondary metal film thickness. Importantly, we also demonstrate that such impermeable microcapsule metal shells can be remotely fractured using ultrasound-based devices that are commensurate with technologies currently used in medical applications, which demonstrate the possibility to adapt these microcapsules for the delivery of cytotoxic drugs.

INTRODUCTION: Microencapsulation of functional materials and chemically or biologically active ingredients is an area of current interest for use in a large range of formulated products. This is due to its wide range of applications in a number of industries such as pharmaceuticals,[1] cosmetics,[2] food and beverages,[3] agrochemicals,[4] textiles,[5] fragrances,[6,7] and oil recovery[8] amongst others.

The main roles of encapsulation are to isolate the active material from its surroundings, act as a form of protection from exterior environments and provide a mechanism for controlled release. Encapsulation can increase the stability and life of the product. For example, active ingredients in the food and pharmaceutical industries can be protected from oxidation or moisture. Encapsulation can facilitate the manipulation of the product during processing. Liquid active components can be converted into a dry solid system and handling properties of sticky materials can be improved. Incompatible components can be separated, which can be beneficial to the food and beverage industries as loss of ingredients during processing can be reduced or avoided and reactive compounds can be separated. [9] Volatile compounds can be encapsulated to retard the

2

release, such as fragrance oils which tend to evaporate quickly.[10] Pesticide formulations can be encapsulated to make it safer for applicators to mix and apply highly toxic materials.[11]

When successful active protection and retention within the designed capsule is obtained, the active release can be sustained over a period of time or triggered by an external stimuli such as change in pH, temperature, light, ultrasound, pressure, chemical or biological environment, electric or magnetic field, depending on the final use.[12,13] For example, pharmaceutical ingredients can be protected from harsh acidic environments in the stomach, and their release delayed until a milder environment has been reached.[14] Targeted release of drugs is particularly beneficial as it can avoid damage to unhealthy tissue and therefore reduce unwanted side effects.[15] Targeted drug delivery also offers a higher therapeutic index and specificity compared to conventional drugs.[16] Very importantly, pharmaceutical active ingredients are often low molecular weight molecules (typically < 500 Da), which offer a significant challenge in simultaneously achieving effective retention within the microcapsule core and triggered release. Indeed, current microcapsule designs, which typically also contain small payloads, tend to leach out some of their contents when in a fully formulated product, or when diluted. These drawbacks often lead to a lower than optimal dosage being delivered to the target site. Alternatives such as liposome/polymersome-based systems have shown good promise in retention but their encapsulation efficiency tends to be poor.[17] This drawback and potential stability issues have severely limited the uptake of these drug delivery alternatives into industry. The relative ease of microcapsule manufacturing and the possibility of loading the active ingredient directly into their core (thus preventing significant loss) is a key requirement for industry adoption. However, 100% EE in microcapsules is still rarely achieved and methods used to improve active retention sometimes involve the use of unfavourable solvents such as dichloromethane[18] or specialised polymers [19] that may be difficult to integrate within tightly regulated product compositions. Hence, a microcapsule system that achieves a) full retention of small actives without leaching over relevant time scales, b) high stability over a wide range of conditions (e.g. full product formulation, dilution, storage, final application conditions such as a biological environment) and c) remote triggering of the payload release is highly desirable.

In addressing the first challenge, permeation of the active ingredients through microcapsule shells, is typically a significant obstacle when encapsulating low molecular weight actives. When considering a microcapsule shell, acting as a barrier for diffusion outside the microcapsule, permeation is dependent upon the active partition into the shell and its diffusion through it.[20,21] It is also a function of the chemical potential imbalance in the system as a result of concentration differences of the active between the core and the continuous phase, the total exposed surface area and thickness of the shell (more details about relating the properties of the microcapsule shells to the release characteristics can be found elsewhere[22-24]). The latter two parameters can be manipulated easily for a set microcapsule system and provide some degree of permeation control. However, one of the prominent challenges of encapsulating small compounds (less than 250 g.mol^{-1}), such as those commonly used in drugs, vitamins, fragrance and flavour oils is the low ratio of active ingredient size as compared to the microcapsule shell pore size, particularly when using polymeric shells. The resulting rapid permeation of such species through polymer membranes leads to a difficulty in controlling leaching of the encapsulated active ingredient thus increasing wastage and possibly undesired side effects. In this case, manipulating the shell thickness or the microcapsule surface area is not sufficient and materials with different partition coefficient or pore sizes must be used to form the microcapsule shell.

As far as the authors are aware, few possible solutions to these problems have been demonstrated thus far.[25] Firstly, microcapsule shells have been designed to force the partition coefficient of an active ingredient largely in favour of the core to prevent leaching.[19, 26, 27] The most recent example of such microcapsules possess fluorinated polymer shells created in a microfluidic environment from double emulsion templates, where the middle oil phase consisting of a fluorinated monomer is polymerised via UV.[19] The resulting capsules were shown to prevent leaching of very small species, including electrolytes and dyes over weeks as a result of their very low partitioning into the shell. Slow leaching was further induced by using solvents that partially swell the shell as the continuous phase. Secondly, some inorganic materials can be used to provide shells with lower porosity. In particular, we have recently demonstrated the possibility of depositing metallic shells onto polymeric microcapsules using electroless deposition as a method for preventing diffusion of small molecular weight oil cores into a continuous phase in which they dissolve with release of the oil cores made possible via mechanical fracture of the shell.[28,29] These metal coating procedures,

however, still require washing steps to remove the excess of catalytic nanoparticles used in the electroless deposition process and still rely on preparing polymer-shell microcapsules as a first step. In addition, release of the core has only been demonstrated via mechanical fracture contact made with the microcapsules, thus limiting their application. However, it is worth noting that noble metal surfaces, in particular gold, have been previously used as suitable materials for systemic drug delivery applications as they tend to be biologically inert and can be modified with biocompatible species routinely.[30]

Here, we describe a method where the metallic film is deposited directly onto an emulsion droplet, hence allowing complete retention of the emulsion core (potentially corresponding to 100% of the active material depending on applications) in the capsule and eliminating waste solvent. As far as the authors are aware, this is the first time that a continuous thin metal film is directly coated onto emulsion droplets via an electroless deposition process. In this process, catalytic platinum nanoparticles are used both as a stabiliser for the oil-in-water emulsion and as the catalyst for the electroless deposition of a complete thin gold film[31] (**Error! Reference source not found.**).
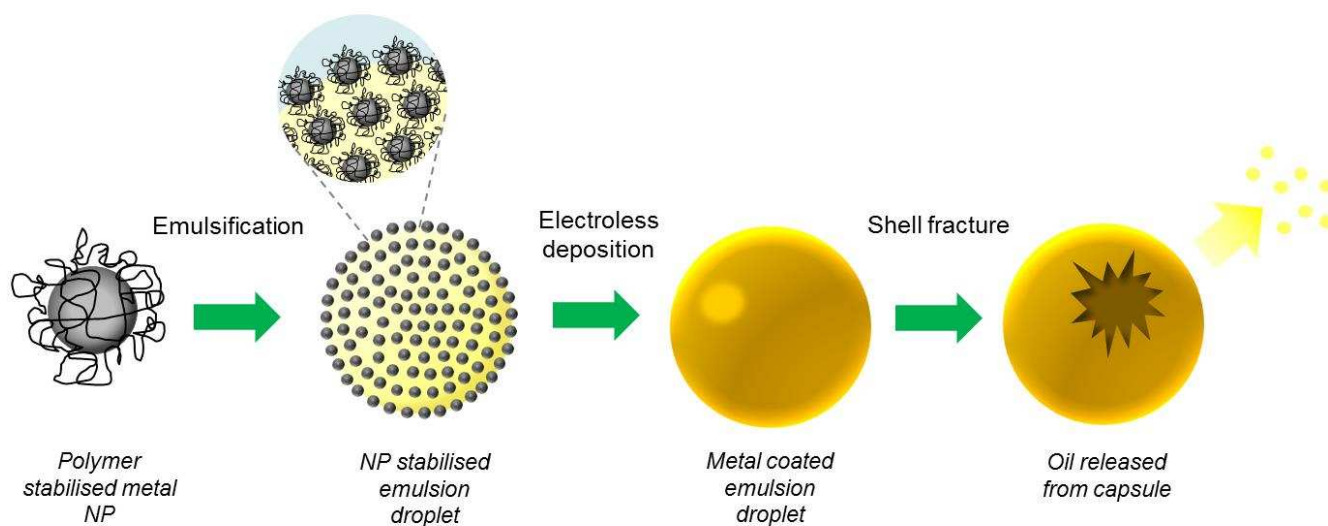

Figure 1: Synthetic route to create a continuous metal film onto an oil droplet via stabilisation of an oil-in-water emulsion with catalytic nanoparticles followed by an electroless deposition process leading to the permanent encapsulation of the oil core. Encapsulated active can be released via remote fracture of the metallic shell using ultrasound.

This work expands our previous studies[28,29b] and develops for the first time a simple two-step method to synthesise microcapsules by coating a thin metal shell onto the surface of emulsion droplets via electroless deposition to encapsulate the entire volume of the precursor emulsion droplets and indefinitely retain the core in an environment that can otherwise rapidly dissolve the droplets. We also subsequently demonstrate that these metal-shell microcapsules can be remotely fractured to release their content using ultrasound at frequencies and intensities suitable for medical applications.

Experimental

Materials

The following chemicals were used as received: poly(vinyl pyrrolidone) (PVP, 40kDa, Fluka Analytical), sodium borohydride (NaBH$_4$, Sigma Aldrich, $\geqslant$98.0%), chloroplatinic acid hydrate (H$_2$PtCl$_6$•H$_2$0, Sigma Aldrich, $\geqslant$99.9% trace metals basis), gold (III) chloride hydrate (HAuCl$_4$•3H$_2$O, Sigma Aldrich, 99.999% trace metals basis), hexadecane (CH$_3$(CH$_2$)$_{14}$CH$_3$, Sigma Aldrich, 99%), hydrochloric acid (fuming HCl, Merck, 37% HCl), hydrogen peroxide (30.5wt% H$_2$O$_2$). Water used in the experiments was purified Millipore Milli-Q water (18.2 MΩ.cm resistivity at 25°C).

Methods

Platinum Nanoparticle (Pt-NPs) synthesis

Pt nanoparticles were synthesised by the reduction of a metal salt in the presence of a reducing agent at room temperature. H$_2$PtCl$_6$-6H$_2$O (0.23 g, 5.61 mM) was dissolved in a 0.0067 wt% PVP solution (100 ml) in a 250 ml conical flask. Under vigorous stirring at 750 rpm using a magnetic bar, NaBH$_4$ (2 ml, 1.1 mM) was rapidly added into the mixture, producing a dark brown solution indicating the formation of platinum nanoparticles (**Error! Reference source not found.**1). After stirring for 20 minutes the nanoparticle suspension was filtered using a 0.2 µm syringe filter and subsequently stored at 5°C prior to use.

$$NaBH_4 + H_2PtCl_6 + 3H_2O \rightarrow Pt + H_3BO_3 + 5HCl + NaCl + 2H_2 \qquad \text{Equation 1}$$
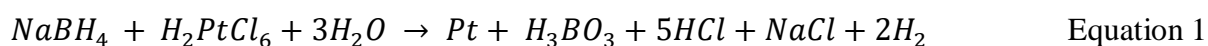
Emulsification of hexadecane with the Pt NPs aqueous suspension

Hexadecane (0.75 ml) was added to the Pt-NPs dispersion (10 ml) and homogenised using a sonic dismembrator ultrasonic processor (Fisher Scientific, Fisherbrand - FB505) for 1 min (40% amplitude) in an ice bath to avoid dramatic increase of the sample temperature. The resulting emulsion was agitated on a carousel for 30 min to allow for limited coalescence of the emulsion droplets to occur. Subsequently the emulsion was washed with Milli-Q water 3 times, once a fully creamed emulsion was obtained.

The larger emulsion droplets used in the experiments demonstrating ultrasound-driven metal shell fracture were synthesised as follows; 4mL of the Pt-NPs dispersion was homogenised with 2 mL of hexadecane using an IKA T25 Digital Ultra Turrax at 24,000 rpm for 2 min. The prepared emulsion was then agitated on a carousel for 30 min. The emulsion was then washed 3 times, each time the bulk phase below the creamed layer was removed and the samples topped up with 10mL of Milli-Q water.

Gold film deposition via electroless plating

The created emulsion of hexadecane stabilised with Pt-NPs (0.75 mL) was added to a plating solution consisting of PVP (5 mL, 0.2 wt% - present here to facilitate stabilisation of the capsules resulting from the reduction reaction), Milli-Q water (10 mL), $HAuCl_4$ (2 mL, 180 mM), and H_2O_2 (1 mL, 1.62 M) to initiate the electroless deposition process. The metal salt reduction reaction (equation 2) occurred very rapidly upon addition of the emulsion sample as a result of the presence of Pt-NPs at the oil-water interface. Within 30s, all characteristic yellow colour from the gold salt had disappeared.

$$2HAuCl_4 + 3H_2O_2 \underset{Pt}{\rightarrow} 2Au + 3O_2 + 8HCl$$
<div align="right">Equation 2</div>
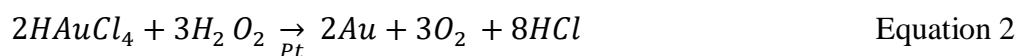
The metal-shell capsules were then agitated on the carousel for 30 mins to allow for the PVP adsorption process to occur thus ensuring colloidal stability of the resulting microcapsules. The microcapsules were subsequently washed by removing the supernatant and replacing with Milli-Q water.

For the experiments where the gold salt concentration was varied the following plating solution was used: Water (10 mL), PVP (10 mL, 0.05 wt%, 67 kDa), $HAuCl_4$ (2 mL) and H_2O_2 (1 mL). The concentration of

HAuCl$_4$ added was varied from 180 mM to 12.5 mM. The ratio of gold salt and reducing agent remained constant for each sample (4.5 x molar excess to ensure full reduction of the metal salt in the process).

The larger metal coated emulsion droplets used in the experiments demonstrating ultrasound-driven metal shell fracture were synthesised as follows: 0.5 mL of the emulsion (described in the emulsification section above) was added to a plating solution containing; water (10 mL), PVP (2 mL, 0.2 wt%, 40 kDa), HAuCl$_4$ (0.25 mL, 100 mM) and H$_2$O$_2$ (1 mL) and was gently stirred for 2 minutes.

Characterisation

Transmission Electron Microscopy (TEM)

Samples were analysed using a FEI Tecnai TF20 field emission transmission gun electron microscope (FEGTEM) fitted with a HAADF detector and Gatan Orius SC600A CCD camera. An Oxford Instruments INCA 350 EDX system/80mm X-Max SDD detector was used for elemental mapping. Prior to analysis, samples were dispersed on a TEM grid (holey carbon film, 400 Cu Mesh from Agar Scientific) and allowed to dry. Particle sizes were then determined using ImageJ software.

Imaging Flow Cytometry

Droplet size distribution was measured using the Benchtop C70 Series FlowCAM imaging flow cytometry instrument, which measures particle size and shape using image analysis. The FlowCAM analyses samples in suspension in real time, therefore allowing information on parameters such as particle size distribution and shape parameters to be calculated simultaneously. The sample is drawn into the flow chamber by a syringe pump and then deposited into an outflow collection. A flash LED light illuminates the chamber, which is then imaged with the objective onto the high-resolution digital camera.

Experiments were recorded in AutoImage mode using a 20x objective, FC50 flow cell in a reverse flow configuration. Post capture, the droplet images were processed with VisualSpreadsheet software using several parameters such as edge gradient, circularity and circle fit to ensure that the droplets used to determine the overall size distribution were in full focus. The size distribution was determined from the

ABD diameter, which corresponds to the total area of all pixels deemed to form part of the particle on the microscopy images.

Gas Chromatograpy (GC)

Release of hexadecane was measured using gas chromatography. 2 mL of the gold coated capsule solution was added to 8 mL absolute ethanol. The capsules were re-dispersed and 1.5 mL sample (x2) was centrifuged at 7000 rpm for 1 min to remove the capsules. The remaining supernatant was added to a GC sample vial for GC analysis. The remaining sample was placed in a water bath at 40 °C. A 1.5 mL sample was taken at 7 days and the previous sampling method repeated.

Samples were run on a Perkin Elmer Clarus 580GC using the following method and column:

GC column: Elite-1 capillary column, length 30 m, internal diameter 0.25 mm. The column temperature was programmed to ramp from 50 °C to 300 °C at 20 °C/min at a flow rate of 2 mL/min.

Nanoparticle density at droplet interface

The density of nanoparticles at the o/w interface was calculated by measuring light transmittance the aqueous phase after the emulsion has creamed and using a calibration to calculate the concentration of NPs remaining in the aqueous phase and thus how many are at the interface.

The particle concentration in the aqueous phase was monitored using a LUMiSizer Dispersion Analyser by measuring the light transmission across the sample under centrifugation (to ensure that only the Pt-NPs in the continuous phase was accounted for to determine their concentration). The intensity of the light transmitted through the sample was recorded at 25°C and at 300rpm using 2mm PC 110-131XX cells at 865nm. First, a calibration curve was obtained for Pt NP samples over a large range of concentrations and all measured transmitted light intensities for each unknown sample was compared against the calibration curve to determine the Pt NP concentration.

Thermo-Gravimetric Analysis (TGA) measurement of metal shell to oil core mass ratio

A dry sample of microcapsules with a known mass was placed in an aluminium crucible with a perforated lid to allow for release of any pressure build up during measurement. The crucible was sealed using a press

machine and placed in the TGA tray to conduct the experiment. The microcapsule sample was heated from 35°C to 105°C (rate 10°C/min) and held for 10 min at 105°C to remove the remaining water present in the sample. The sample temperature was subsequently ramped up to 500°C (rate 10°C/min) to remove the hexadecane core. The remaining mass was thus taken as the mass of metal in the sample. The size distribution of the microcapsules was then used to calculate a total microcapsule surface area, which was then used as a basis for determining metal shell thickness of the capsules based on the measured oil core/metal mass ratio.

Atomic Force Microscopy (AFM) measurement of microcapsule shell thickness

Atomic force microscopy (AFM) (Veeco BioScope 2) was used to characterise metal film thickness and morphology. Thin shell capsules were observed to collapse upon drying in air. Thus for AFM measurements the thin metal-shell microcapsules were dried on glass slides and ethanol was subsequently micro-pipetted onto the slide to displace (and then remove) the remaining organic core phase. The sample was then imaged and single wall films were sought out to conduct height profile measurements. Thicker shelled capsules, which did not readily collapse when dry, were first broken using an ultrasound probe head (20seconds at 30% power) and then washed by centrifuge in ethanol, deposited on glass slides and height profiled.

Ultrasound-based remote fracture of microcapsule shell

A 1.1 MHz high intensity focused ultrasound (HIFU) transducer (H102, Sonic Concepts, USA) driven by a power amplifier (A300, E&I, USA) and function generator (33250A, Agilent Keysight, USA) was used. The free field acoustic pressure output of the transducer was measured using a National Physical Laboratory (NPL) calibrated membrane hydrophone. An acoustic pulse with a 6 MPa peak positive and 4.5 MPa peak negative pressure was used to fracture the microcapsule shells. The total exposure time (s), peak acoustic pressure (MPa) and burst cycles were controlled using a custom Matlab (Mathworks Ind, USA) program. For this study, the number of acoustic cycles in each HIFU burst applied onto the flowing capsule suspension was varied between 0-30 cycles, using a 0.5 Hz pulse repetition frequency, for a total exposure duration of 80 s. In order to record the proportion of fractured microcapsules for each cycle of applied ultrasound energy; stills were extracted from a continuous video of the process immediately after each pulse.

Images were then manually analysed to count the percentage of capsules with fractured metal films within a constant area (see supplementary data (figure S5) for further explanation of how the stills were manually analysed).

Results and Discussion

Synthesis of PVP-stabilised platinum nanoparticles (Pt-NPs)

Metal nanoparticles have been widely reported for their use as catalysts. They offer the advantage of a high surface-to-volume ratio due to their small size and can also be designed to have good dispersion stability, which enhances their effectiveness as compared to larger crystals.[32,33] Interestingly for this work, it has been shown that metal NPs are able to preferentially direct the growth of a secondary metal (both when suspended in a continuous phase and when adsorbed on a solid substrate) through reduction of the corresponding salt. For example, Horiuchi et al.[31] demonstrated the growth of a gold film on a surface covered with platinum nanoparticles (Pt-NPs). In their work, the Pt-NPs were synthesised in the presence of poly(vinyl pyrrolidone) (PVP), which provides steric stabilisation to the nanoparticles and which was not seen to influence the catalytic activity of the substrate. The procedure developed here for synthesising Pt-NPs sterically stabilised by PVP was therefore adapted from this previous work.

In most previous studies where a polymer stabiliser is used in the synthesis of metal nanoparticles, a large excess of polymer chains is typically used to enable rapid and efficient polymer coverage on the particle surface, thus enabling long-term stability.[34] However, when the nanoparticles are subsequently adsorbed onto a solid substrate, often as a way of immobilising a catalyst, the excess polymer in the bulk can compete for surface adsorption sites and can significantly reduce the efficiency of the adsorption process and the final catalyst density on the surface.[34] Thus, in this work, the PVP stabiliser concentration in the nanoparticle synthesis was purposefully minimised to enhance the subsequent nanoparticle surface densities upon the subsequent interfacial adsorption process, while retaining short-term stability (at least 30 days at 5°C). Figure 2a shows a representative transmission electron micrograph of the synthesised Pt-NPs, demonstrating good control over particle size and polydispersity achieved with the developed synthesis procedure.
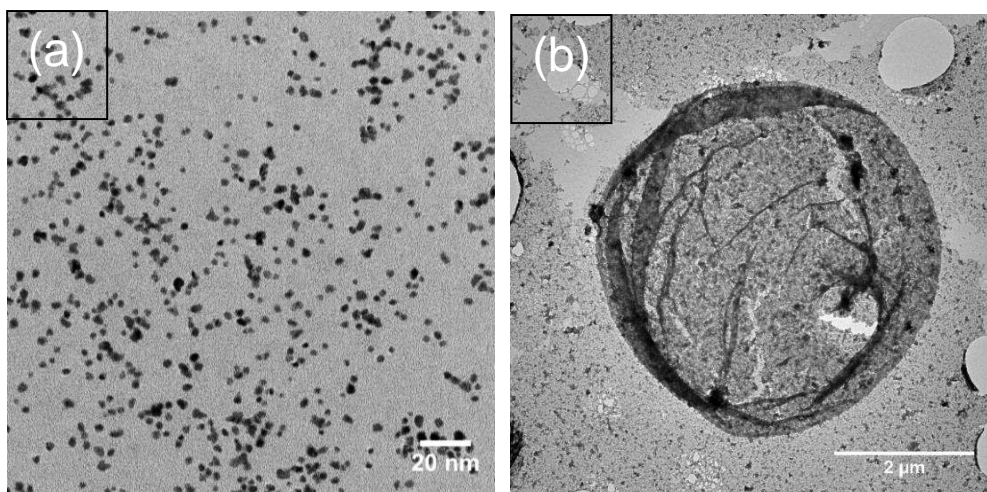
Figure 2: a) Transmission Electron Micrograph of PVP-stabilised Pt nanoparticles (Pt-NPs) as prepared using an optimised concentration of PVP in the synthesis to minimise excess polymer in the bulk; and b) Transmission Electron Micrograph of a representative nanoparticle film after drying of the corresponding emulsion droplet following adsorption of the Pt-NPs at the oil/water interface during the emulsification step.

Emulsification of hexadecane in the Pt-NPs aqueous suspension

Hexadecane was used as a model oil in the emulsification process, where the Pt-NPs aqueous dispersion was mixed with different oil volume fractions and subsequently emulsified using an ultrasonic probe. The Pt-NPs efficiently adsorbed to the interface, leading to stable emulsions suggesting a suitable three-phase contact angle for the particles to warrant strong adsorption at this oil-water interface. Adsorption of metal nanoparticles at oil-water interfaces have been studied before and our data here seem to agree well with the propensity for such nanoparticles to be present at such interfaces.[35,36,37] It is also worth noting that upon drying the emulsions on a solid substrate, the nanoparticle film did not break and a resulting nanoparticle 'membrane' could be observed using electron microscopy in the position where the emulsion droplets settled (Figure 2b). This observation suggests that the polymer stabiliser on the surface of the Pt-NPs may entangle at the oil-water interface between adjacent nanoparticles thus creating an elastic film around the droplets as often observed in other studies when polymer stabilisers are cross-linked.[38],[39] This phenomenon has also been noticed before in other systems containing PVP as a stabiliser[40] and we hypothesize that it contributes to enhancing the emulsion stability.

Several different parameters are involved in controlling the emulsification process and the resulting size and stability of the emulsion droplets, including the oil/water volume fraction, the nanoparticle concentration, the presence of excess free PVP in the bulk[34] and the energy input for the emulsification. Investigating these parameters in detail is beyond the scope of this work. However, we briefly exemplify here our ability to control the emulsion properties through the change of one particular parameter during the emulsification process, namely the ratio of oil to water. This ratio was varied to control the amount of interface created during the emulsification process while energy input and nanoparticle concentration were kept constant. This is particularly important for the process of creating a dense metal film on the emulsion droplets via electroless deposition, as varying the amount of oil/water interface can help control the level of excess nanoparticles in the bulk of the produced emulsion. For this particular emulsion system stabilised solely by the Pt-NPs, increasing the ratio of oil to water resulted in an increase in the size and polydispersity of the droplets as shown in Figure 3.
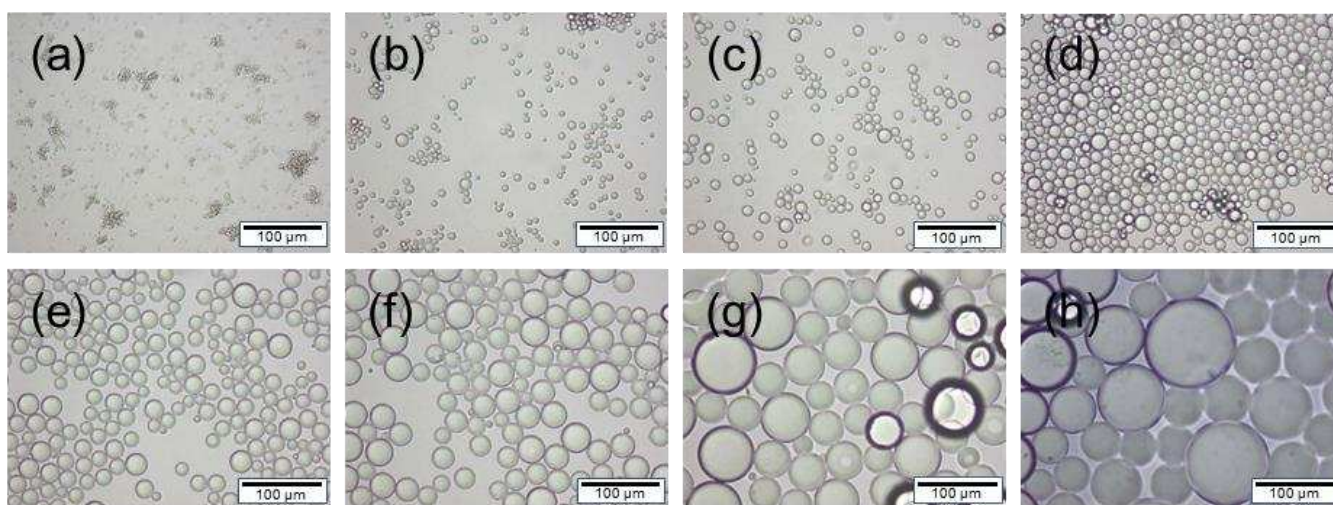

Figure 3: Optical micrographs of emulsions prepared with different oil volume fractions; (a) 0.01, (b) 0.05, (c) 0.07, (d) 0.09, (e) 0.13, (f) 0.17, (g) 0.23, (h) 0.29vol%, respectively. Hexadecane and Pt-NPs dispersions (10 mL) were homogenised at 40 % amplitude for 1 min on an ultrasonic processor. Scale bar = 100 µm. Note that the sample with highest oil volume fraction (0.29vol%) coalesced rapidly and thus was not included in the following studies.

Droplet diameter distribution for each sample was measured over the range of prepared emulsions and the corresponding data are plotted in Figure 4. The droplet diameter distributions were also used to calculate the total interfacial area stabilised by the nanoparticles for each oil volume fraction. The nanoparticle concentration remaining in the bulk after emulsification (i.e. not adsorbed at the oil/water interface) was characterised using light transmittance measurements (as described in the experimental section) after full creaming of the emulsion droplets. On that basis, it was then possible to predict an average nanoparticle density on the emulsion droplet surface for each of the prepared emulsion samples by assuming that a) all oil was successfully emulsified and b) the nanoparticles were arranged in a close packed hexagonal array at the interface. These data are shown in the supplementary information and demonstrate that, as expected, at low oil volume fraction (starting at $\Phi=0.05$) the interface is covered by a dense layer of particles, which likely corresponds to the maximum achievable Pt-NP packing density for this system. As the volume fraction of oil is increased, the total oil-water interfacial area in the system is initially seen to plateau owing to a sufficient number of Pt-NPs present in the continuous phase to sustain a rapid and efficient particle adsorption at the interface. When the oil volume fraction is increased above 0.13% however, the Pt-NPs density at the interface is seen to decrease. At the largest oil volume fraction considered here ($\Phi= 0.23$), the total interfacial area increases drastically and the density of the Pt-NPs at the interface decreases sharply. In addition, this emulsion was seen to be unstable with the presence of coalesced oil at the top of the samples within a few hours, which shows the limit of our initial assumption (i.e. all oil is emulsified in the sample).
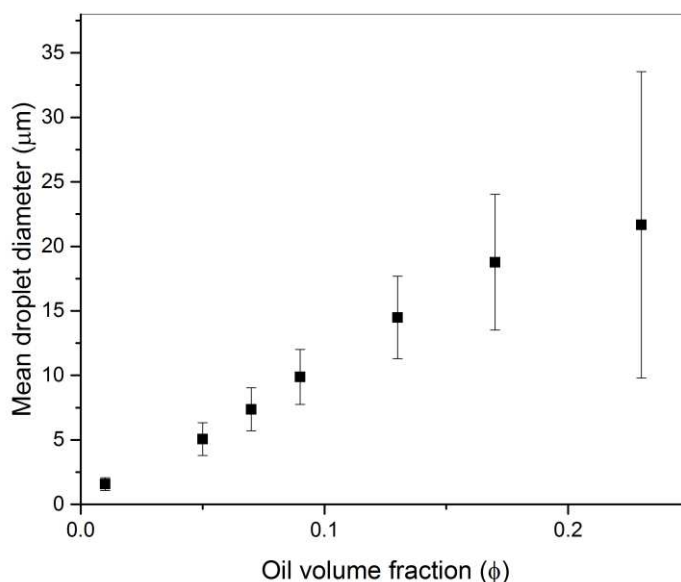
Figure 4: Mean droplet diameter of hexadecane-in-water emulsions stabilised by Pt NPs for increasing oil volume fractions (ϕ). Hexadecane and Pt-NPs dispersions (10 mL) were homogenised at 40 % amplitude for 1 min using an ultrasonic processor. The error bars represent the standard deviation of the mean droplet size as measured with a flow cytometry instrument.

As illustrated in

Figure , the mean diameter increases with increasing oil volume fraction (ϕ). At $\phi = 0.01$ droplet aggregation can be observed, likely as a result of the presence of a large excess of Pt-NPs in the system leading to a depletion flocculation phenomenon.[41] Additionally, it is worth noting that a significant amount of coalescence was observed in the emulsions after creaming for $\phi > 0.23$ (thus these data are not included in these graphs), which suggests that the lower Pt-NPs density at the oil-water interface for high volume fractions results, as expected, in less stable emulsions.

We believe the evolution of the different parameters characterised in Figures 3, 4 and S3 (emulsion droplet size and polydispersity, nanoparticle interfacial coverage) is likely a result of a limited coalescence process, which is a common phenomenon observed for Pickering emulsions.[42,43] In this case, the nanoparticles rapidly cover the newly created interface with the resulting droplets subsequently coalescing until a full coverage of particles is achieved, which imparts colloidal stability to the droplets. This process leads to a

15

final droplet size distribution when full coverage is achieved. As more oil is added to the system, a larger interface is initially created and the droplets have to grow to a larger size to achieve full interfacial coverage. This is verified in our work by the fact that almost all nanoparticles are adsorbed to the oil-water interface (except at the smallest oil volume) and that the total droplet interfacial area, once the system is equilibrated, remains constant (except for the largest oil volumes) and corresponds closely to the theoretical calculation of the total interfacial area the nanoparticles can cover. At the lowest oil volume fractions, the nanoparticles are in excess and some remain in the continuous phase while at the highest oil volume fractions, the nanoparticle concentration is not sufficient to achieve full coverage thus leading to significant droplet instability.

This small initial study of emulsion characteristics as a function of oil fraction allows for tuning the diameter of the droplets produced during emulsification and as a result for subsequent good control of the final microcapsule size in the approximate range of 2 to 25μm. For the following sections, which investigate the deposition of the secondary metal film, an oil volume fraction of $\phi = 0.07$ was chosen as little excess Pt-NPs was present in the bulk in this system and the emulsion retained very good stability.

Electroless deposition of gold films onto Pt-NPs-stabilised emulsion droplets

The Pt-NPs stabilised emulsions were subsequently used as a template for the growth of a thin impermeable metallic film. Previous studies have demonstrated impermeable metal coated microcapsules but the synthesis has typically involved many stages.[23] In this part of the work, we demonstrate that impermeable metal films of the same quality can be obtained using a much simpler metal-shell synthesis process.

Here, the Pt-NPs stabilising the emulsion are also used as a catalyst/nucleus for the electroless deposition of a gold film encapsulating the entire emulsion droplet volume manufactured initially. Importantly, the Pt-NPs limit the reduction of the gold salt to the surface of the emulsion droplets, with only traces of gold growth observed in the bulk as long as all the particles are adsorbed at the oil/water interface during the emulsification process. It is also worth noting that a slight excess of hydrogen peroxide (i.e. a weak reducing agent) is used in this case to ensure all of the gold salt is reacted, thus minimising waste of the most expensive component of the system.

In this part of the work, we prepared different metal-shell microcapsule samples from the same Pt-NPs stabilised emulsion template with increasing gold-film thicknesses. Optical micrographs of the resulting metal-shell microcapsules are presented in Figure 5 for both transmitted light and reflected light observations for three samples as an example (Representative optical micrographs obtained for all samples are presented in Figure S2 in the supplementary information). One characteristic of the microcapsules is the change in light reflection of the samples of different metal-shell thickness and roughness, with the thicker films (e.g. Fig. 5a) leading to rougher and less reflective surfaces while thin metal films (e.g. Fig. 5c) led to smoother, more reflective microcapsule surfaces. Scanning electron micrographs of all three samples are also presented, where the differences in metal shell thickness are obvious from effective mechanical strength shown by each sample within the vacuum chamber of the instrument. The thinnest shell microcapsules are seen to collapse completely under these conditions, while the thickest shell microcapsules are able to maintain their shape after drying.
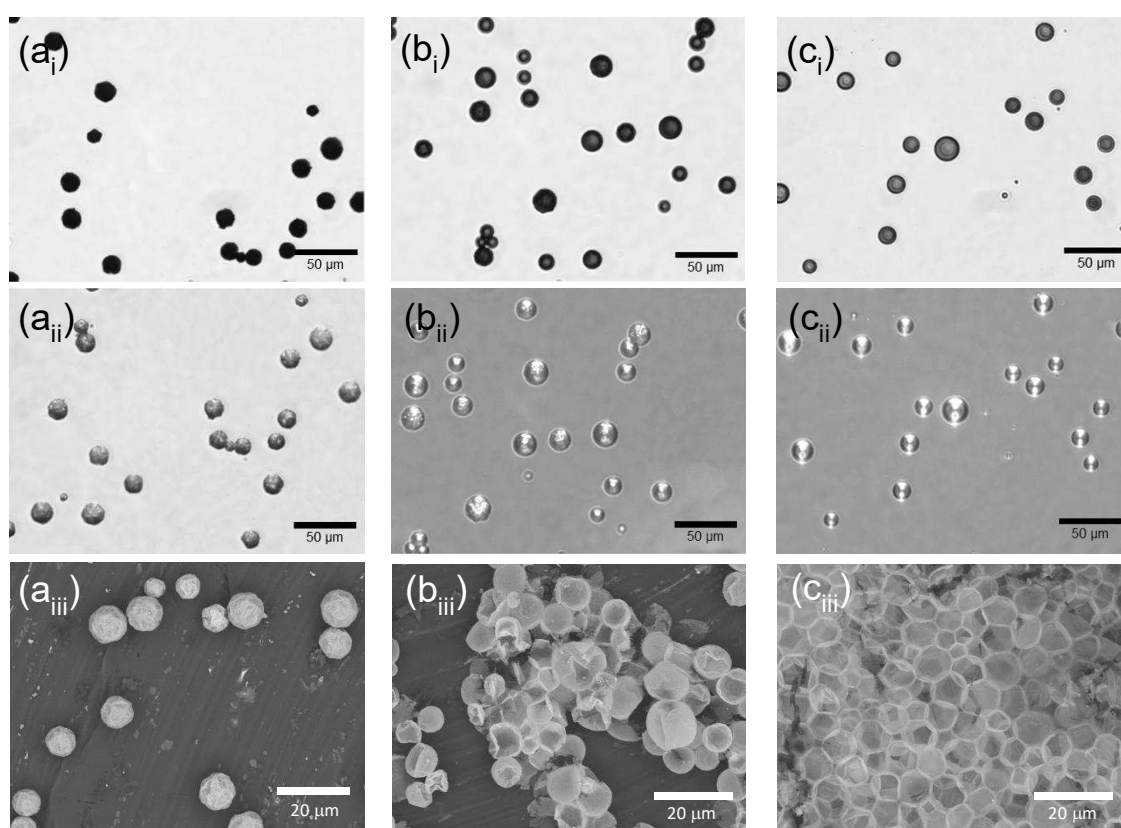

Figure 5: Representative micrographs of gold coated microcapsules prepared with different concentrations of gold salt in the electroless deposition process; (a) 180 mM, (b) 25 mM, and (c) 6.25 mM, respectively.

Micrographs are obtained from an optical microscope in (i) transmitted light, (ii) reflected light and from a scanning electron microscope (iii).

Additionally, very good control over the thickness of the deposited gold film was demonstrated by simply varying the concentration of gold salt used in the emulsion continuous phase (Figure 6). This is particularly useful as it allows for control of the overall metal-shell microcapsule density, optical properties (such as optical resonance)[44,45] and also mechanical stability. The size distribution of the emulsion template used in this case is known, which allows us to calculate the total oil/water interfacial area in the sample and therefore, assuming that all gold salt is reduced and deposited onto the emulsion droplets, to also calculate the metal film thickness and corresponding metal-shell microcapsule density for all six samples. These data are presented in Figure 6 and agree well with the observed microcapsule density difference with the aqueous continuous phase (thicker metal film microcapsules sediment while the thinner metal film microcapsules cream with an intermediate behaviour observed for density close to that of water as a result of the polydispersity of the initial emulsion template). On the basis of these assumptions, the calculated thicknesses for the 6 different samples range from 4 to 122 nm, demonstrating that very thin metal films can be efficiently deposited on the Pt-NPs stabilised emulsion templates. Rapidly creaming/sedimenting microcapsules may only be used within a stabilising (gel or high viscosity dispersion) matrix for topical drug delivery (e.g. in resection cavities after an operation[46]) for example but smaller metal-shell capsules (100nm and below) will be much less influenced by density differences and would be appropriate for use in systemic drug delivery.
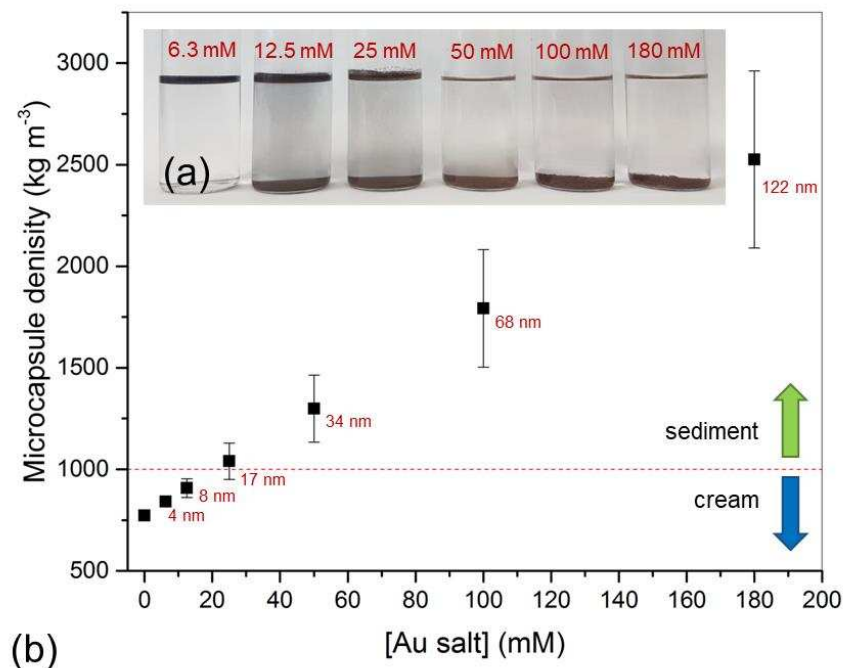
Figure 6: a) Theoretical microcapsule densities as a function of gold salt concentration added to the plating solution. The red line represents the density of water. The value at zero represents the bulk density of the oil core. The annotated numbers indicate the theoretical shell thickness of the microcapsules calculated assuming all gold salt is reduced at the droplet surface and using the total interfacial area derived from the measured particle size distribution. The error bars represent the standard deviation of the mean for all experimental data points. b) Inset - Digital image of the metal-shell microcapsule suspension samples analysed in a), where the synthesis involved increasing concentrations of gold salt (from left to right) for the electroless deposition process on the surface of the emulsion template. The resulting metal-shell microcapsules are seen to cream for the lowest gold salt concentrations (and thus thinnest metal shells) and to sediment for the highest gold salt concentrations (thickest metal shells). The corresponding Au salt concentrations used in the reaction are indicated in red and correspond to the X-axis in a).

As mentioned above, the metal-shell thicknesses and corresponding overall microcapsule density data in Figure 6 are calculated by assuming that all of the gold salt is reduced onto the growing metal film. However, previous studies have suggested that for electroless deposition of gold onto a surface coated with Pt-NPs, the film growth occurs in two separate stages with different growth rates: a rapid initial growth until

all the available Pt surface is covered, and a subsequent slower growth phase on the already deposited gold layer.[47,48,49] Here, we make the assumption that the differences in the growth processes may lead to varying efficiency of gold deposition on the surface and thus attempt to explore this phenomenon. To verify the evolution of the metal shell thickness deposited with increasing gold salt concentration, we conducted further gold shell deposition experiments to explore a broader range of metal shell thicknesses. We then measured the obtained shell thicknesses and compared these data with expected thicknesses assuming all gold is deposited on the droplet surfaces. Firstly, Atomic Force Microscopy (AFM) characterisation of mechanically fractured microcapsule fragments was performed. Height measurements were obtained for all samples, as described in the experimental section, to extract the thickness of the metal shell. Secondly, we also measured the metal to oil core mass ratio using Thermo-Gravimetric Analysis (TGA) for dried samples of the microcapsules and calculated the corresponding metal shell thickness using the measured microcapsule size distribution to infer the total microcapsule surface area. The corresponding data for the range of metal-shell microcapsule samples prepared to explore a broad range of potential metal film thicknesses are presented in Figure 7.
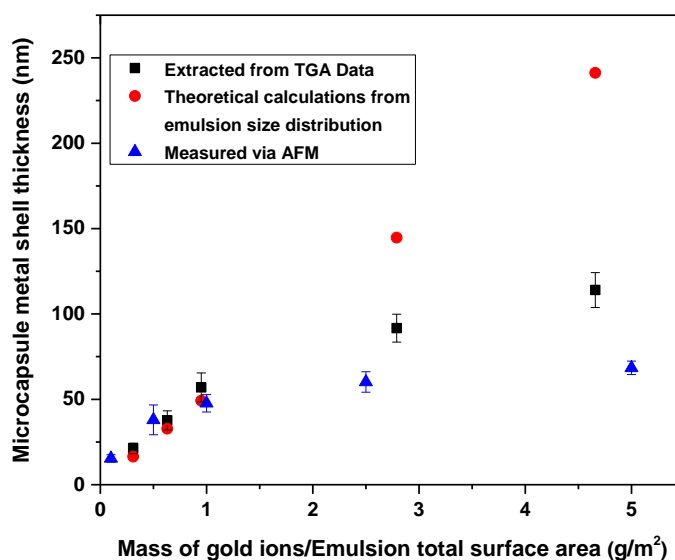

Figure 7: Microcapsule metal shell thickness as a function of increasing ratio between mass of metal ions in the electroless deposition process and total emulsion surface area. The theoretical calculation of the shell thickness assumes all metal ions are reduced and deposited on the emulsion droplets in the electroless

deposition process. Both theoretical and TGA data use the measured emulsion size distribution as a basis for shell thickness calculations while the AFM data give a direct measurement of the shell thickness.

From these data, we can identify two behaviours for the growth of the gold films onto the emulsion droplet surfaces. An initial linear increase in shell thickness is measured at low gold salt concentrations with a reduced rate of increase at higher concentrations. This behaviour is consistent with the previous studies, as the deviation from the linear increase in metal shell thickness at high gold salt concentrations likely results from a second, less efficient, growth phase once all the Pt surface has been covered.
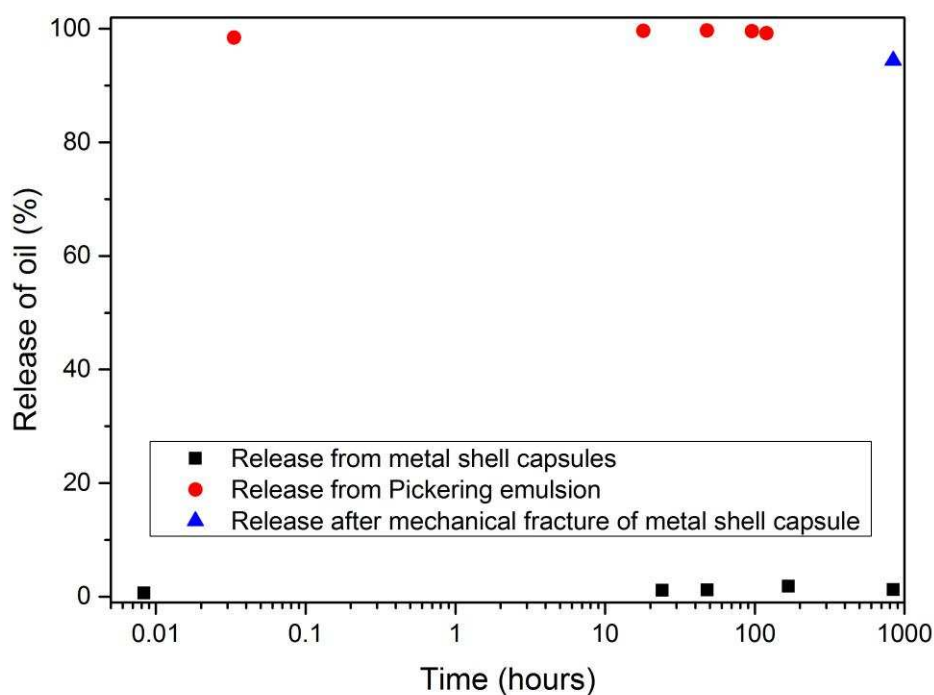

Figure 8: Oil core release experiments conducted for metal-shell microcapsules and their Pt-NP-stabilised emulsion droplet templates. The metal-shell microcapsules were synthesised from the chosen standard Pt-NPs-stabilised emulsion described above with a shell thickness of approximately 50 nm as measured in Figure 7. The release experiments were conducted in a continuous phase of Ethanol:Water in a 4:1 ratio to demonstrate metal-shell capsule impermeability in an environment that dissolves the microcapsule core.

Furthermore, Figure 8 demonstrates that the microcapsules produced by this method can indeed retain their oil core very efficiently within a continuous phase that can dissolve the core, while polymer-shell microcapsules prepared in a previous study[32] leach out all of their core content within minutes in the same continuous phase. The fact that ~ 95% of oil was retrieved from the metal-shell capsules after mechanical fracture further demonstrates successful retention within the metal-shell. In the case where thinner gold shells are deposited on the emulsion droplets, some rapid loss of core oil is not avoided, likely as a result of shell fracture during processing (up to 20% loss for the thinnest shells) but the remaining encapsulated oil is also fully retained for the same time period.

Controlled fracture of metal-shell microcapsules using ultrasound

In the previous sections, we demonstrate a route to produce impermeable microcapsules in a very simple and efficient process. One of the potential applications of such systems is the delivery of highly toxic drugs, for applications such as chemotherapy. To achieve this, a suitable method for activating the release of the drug on demand is required. Thus, we explore the use of ultrasound energy to remotely fracture the metal shell and enable release of the microcapsule cores. Biological cells are largely acoustically transparent at the frequency this device is operated at,[50] which would allow for maximum tissue penetration due to low acoustic attenuation[51] in a medical environment. Figure 9 shows the percentage of metal microcapsules remotely fractured as a function of ultrasound pulse cycle number when passed through a flow cell.
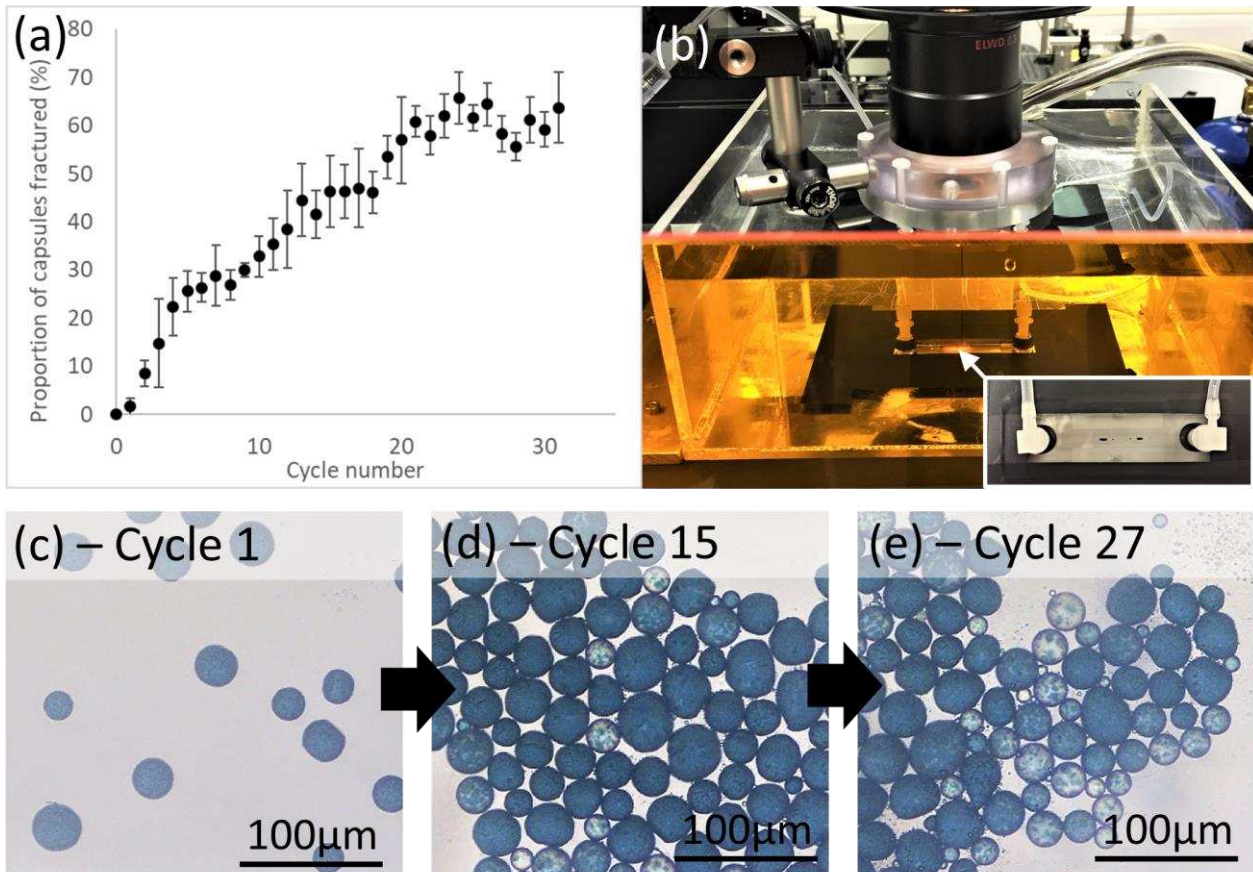
Figure 9: (a) Proportion of metal microcapsules fractured as a function of ultrasound pulse cycle number when passed through a flow cell, (b) ultrasonic assembly used in the process showing the ultrasound transducer head inserted within the water tank – inset: flow cell used to deliver the microcapsules to the transducer. Transducer to flow cell distance ~12cm. Inverted microscope images (c-e) show the microcapsules after being subjected to an increasing number of ultrasound pulse cycles.

Here, we clearly demonstrate the remote fracture of the capsule shells at clinically appropriate ultrasound frequencies (1.1MHz), which indicates that local release of the capsule cores is possible. The proportion of broken capsules was seen to increase with pulse cycle number thereby providing an opportunity for phased release. It should be noted that all capsules were seen to break within 0.5 s in a single ultrasound dose when the duty cycle was increased to 100%.

Conclusion

We have presented a simple method which allows the encapsulation of an oil core via the deposition of a metallic film localised on the droplet interface. The entire process can be carried out at room temperature and does not require the use of harmful solvents used in previous methods, which provides an economical advantage. We have shown control of emulsion droplet size and nanoparticle density at the oil-water interface. Importantly, the gold films that are subsequently deposited on the emulsion droplets were shown to be impermeable and suitable to encapsulate small molecules in challenging environments. Additionally, we have demonstrated that the microcapsule metal shells can be remotely fractured using ultrasound, which opens significant possibilities to control core release for delivering small molecules (in particular cytotoxic drugs) while preventing undesired leaching prior to release activation.

References

1.   Nitika Agnihotri, R. M., Chirag Goda, Manu Arora, Microencapsulation – A Novel Approach in Drug Delivery: A Review. *Indo Global Journal of Pharmaceutical Sciences* **2012,** *2* (1), 1-20.
2.   Illésová, A.; Bučko, M.; Vikartovská, A.; Gemeiner, P., Encapsulation as a useful tool for a biotechnological production of natural aromas. *Current Opinion in Biotechnology* **2013,** *24, Supplement 1* (0), S59-S60.
3.   Gouin, S., Microencapsulation: industrial appraisal of existing technologies and trends. *Trends in Food Science & Technology* **2004,** *15* (7–8), 330-347.
4.   Varona, S.; Kareth, S.; Martin, A.; Cocero, M. J., Formulation of lavandin essential oil with biopolymers by PGSS for application as biocide in ecological agriculture. *J. Supercrit. Fluids* **2010,** *54* (3), 369-377.
5.   Nelson, G., Application of microencapsulation in textiles. *International Journal of Pharmaceutics* **2002,** *242* (1–2), 55-62.
6.   Meyer, A., Perfume Microencapsulation by Complex Coacervation. *CHIMIA International Journal for Chemistry* **1992,** *46* (4), 101-102.
7.   Peña, B.; Panisello, C.; Aresté, G.; Garcia-Valls, R.; Gumí, T., Preparation and characterization of polysulfone microcapsules for perfume release. *Chemical Engineering Journal* **2012,** *179* (0), 394-403.
8.   Keller, B. C., Nanotechnology for spilled oil encapsulation, remediation and recovery. Google Patents: 2011.
9.   Lin, Y.; Skaff, H.; Böker, A.; Dinsmore, A. D.; Emrick, T.; Russell, T. P., Ultrathin Cross-Linked Nanoparticle Membranes. *Journal of the American Chemical Society* **2003,** *125* (42), 12690-12691.
10.   Tekin, R.; Bac, N.; Erdogmus, H., Microencapsulation of Fragrance and Natural Volatile Oils for Application in Cosmetics, and Household Cleaning Products. *Macromolecular Symposia* **2013,** *333* (1), 35-40.
11.   Whithaus, S. M.; Blecker, L., *The Safe and Effective Use of Pesticides, 3rd Edition*. University of California Agriculture and Natural Resources: 2016.
12.   Esser-Kahn, A. P.; Odom, S. A.; Sottos, N. R.; White, S. R.; Moore, J. S., Triggered release from polymer capsules. *Macromolecules* **2011,** *44* (14), 5539-5553.
13.   Klibanov, A. L.; Shevchenko, T. I.; Raju, B. I.; Seip, R.; Chin, C. T., Ultrasound-triggered release of materials entrapped in microbubble–liposome constructs: a tool for targeted drug delivery. *Journal of controlled release* **2010,** *148* (1), 13-17.

14.   San Miguel, A.; Scrimgeour, J.; Curtis, J. E.; Behrens, S. H., Smart colloidosomes with a dissolution trigger. *Soft Matter* **2010,** *6* (14), 3163-3166.

15.   Dromi, S.; Frenkel, V.; Luk, A.; Traughber, B.; Angstadt, M.; Bur, M.; Poff, J.; Xie, J.; Libutti, S. K.; Li, K. C., Pulsed-high intensity focused ultrasound and low temperature–sensitive liposomes for enhanced targeted drug delivery and antitumor effect. *Clinical Cancer Research* **2007,** *13* (9), 2722-2727.

16.   Rani, K.; Paliwal, S., A review on targeted drug delivery: Its entire focus on advanced therapeutics and diagnostics. *Sch. J. App. Med. Sci* **2014,** *2* (1C), 328-331.

17.   Eloy, J. O.; de Souza, M. C.; Petrilli, R.; Barcellos, J. P. A.; Lee, R. J.; Marchetti, J. M., Liposomes as carriers of hydrophilic small molecule drugs: strategies to enhance encapsulation and delivery. *Colloids and surfaces B: Biointerfaces* **2014,** *123*, 345-363.

18.   Ramazani, F.; Chen, W.; van Nostrum, C. F.; Storm, G.; Kiessling, F.; Lammers, T.; Hennink, W. E.; Kok, R. J., Strategies for encapsulation of small hydrophilic and amphiphilic drugs in PLGA microspheres: State-of-the-art and challenges. *International Journal of Pharmaceutics* **2016,** *499* (1–2), 358-367.

19.   Zieringer, M. A.; Carroll, N. J.; Abbaspourrad, A.; Koehler, S. A.; Weitz, D. A., Microcapsules for enhanced cargo retention and diversity. *Small* **2015,** *11* (24), 2903-2909.

20.   Gaonkar, A. G.; Vasisht, N.; Khare, A. R.; Sobel, R., *Microencapsulation in the food industry: a practical implementation guide*. Elsevier: 2014.

21.   Mishra, M., *Handbook of Encapsulation and Controlled Release*. CRC Press: 2015.

22.   Trojer, M. A.; Nordstierna, L.; Nordin, M.; Nydén, M.; Holmberg, K., Encapsulation of actives for sustained release. *Physical Chemistry Chemical Physics* **2013,** *15* (41), 17727-17741.

23.   Richards, J. H., The role of polymer permeability in the control of drug release. In *Polymer Permeability*, Springer: 1985; pp 217-267.

24.   Trojer, M. A., Polymeric Core-Shell Particles: Physicochemical Properties and Controlled Release in Encyclopedia of Surface and Colloid Science, ed. P. Somasundaran. Taylor and Francis, New York: 2013.

25.   Latnikova, A.; Jobmann, M., Towards Microcapsules with Improved Barrier Properties. *Topics in Current Chemistry* **2017,** *375* (3), 64.

26.   Antipov, A. A.; Sukhorukov, G. B.; Donath, E.; Möhwald, H., Sustained release properties of polyelectrolyte multilayer capsules. *The Journal of Physical Chemistry B* **2001,** *105* (12), 2281-2284.

27.   Trojer, M. A.; Andersson, H.; Li, Y.; Borg, J.; Holmberg, K.; Nydén, M.; Nordstierna, L., Charged microcapsules for controlled release of hydrophobic actives. Part III: the effect of polyelectrolyte brush-and multilayers on sustained release. *Physical Chemistry Chemical Physics* **2013,** *15* (17), 6456-6466.

28.   Hitchcock, J. P.; Tasker, A. L.; Baxter, E. A.; Biggs, S.; Cayre, O. J., Long-term retention of small, volatile molecular species within metallic microcapsules. *ACS Applied Materials & Interfaces* **2015,** *7* (27), 14808-14815.

29.   (a) Tasker, A. L.; Hitchcock, J.; Baxter, E. A.; Cayre, D. O. J.; Biggs, S., Understanding the mechanisms of gold shell growth onto polymer microcapsules to control shell thickness. *Chemistry–An Asian Journal* **2017,** *12* (13), 1641-1648; (b) Tasker, A. L.; Puttick, S.; Hitchcock, J.; Cayre, O. J.; Blakey, I.; Whittaker, A. K.; Biggs, S., A two-step synthesis for preparing metal microcapsules with a biodegradable polymer substrate. *Journal of Materials Chemistry B* **2018,** *6* (14), 2151-2158.

30.   Ghosh, P.; Han, G.; De, M.; Kim, C. K.; Rotello, V. M., Gold nanoparticles in delivery applications. *Advanced drug delivery reviews* **2008,** *60* (11), 1307-1315.

31.   Horiuchi, S.; Nakao, Y., Platinum colloid catalyzed etchingless gold electroless plating with strong adhesion to polymers. *Surface and Coatings Technology* **2010,** *204* (23), 3811-3817.

32.   (a) Roldan Cuenya, B., Metal Nanoparticle Catalysts Beginning to Shape-up. *Accounts of Chemical Research* **2012,** *46* (8), 1682-1691; (b) Hvolbæk, B.; Janssens, T. V. W.; Clausen, B. S.; Falsig, H.; Christensen, C. H.; Nørskov, J. K., Catalytic activity of Au nanoparticles. *Nano Today* **2007,** *2* (4), 14-18.

33.   Moshfegh, A. Z., Nanoparticle catalysts. *Journal of Physics D: Applied Physics* **2009,** *42* (23), 233001.

34.   Hitchcock, J. P.; Tasker, A. L.; Stark, K.; Leeson, A.; Baxter, E. A.; Biggs, S.; Cayre, O. J., Adsorption of catalytic nanoparticles onto polymer substrates for controlled deposition of microcapsule metal shells. *Langmuir* **2018,** *34* (4), 1473-1480.

35.   Booth, S. G.; Alghamdi, R. G.; Belić, D.; Brust, M., Electrodeposition of Gold Nanostructures at the Interface of a Pickering Emulsion. *ChemElectroChem* **2018,** *5* (15), 2055-2058.

36.   Sachdev, S.; Maugi, R.; Woolley, J.; Kirk, C.; Zhou, Z.; Christie, S. D. R.; Platt, M., Synthesis of Gold Nanoparticles Using the Interface of an Emulsion Droplet. *Langmuir* **2017,** *33* (22), 5464-5472.

37.   Smirnov, E.; Scanlon, M. D.; Momotenko, D.; Vrubel, H.; Méndez, M. A.; Brevet, P.-F.; Girault, H. H., Gold Metal Liquid-Like Droplets. *ACS Nano* **2014,** *8* (9), 9471-9481.

38.   Yuan, Q.; Cayre, O. J.; Fujii, S.; Armes, S. P.; Williams, R. A.; Biggs, S., Responsive Core–Shell Latex Particles as Colloidosome Microcapsule Membranes. *Langmuir* **2010,** *26* (23), 18408-18414.

39.   Thompson, K. L.; Armes, S. P., From well-defined macromonomers to sterically-stabilised latexes to covalently cross-linkable colloidosomes: exerting control over multiple length scales. *Chemical Communications* **2010,** *46* (29), 5274-5276.

40.   Yu, K.; Zhang, H.; Hodges, C.; Biggs, S.; Xu, Z.; Cayre, O. J.; Harbottle, D., Foaming Behavior of Polymer-Coated Colloids: The Need for Thick Liquid Films. *Langmuir* **2017,** *33* (26), 6528-6539.

41.   (a) Jenkins, P.; Snowden, M., Depletion flocculation in colloidal dispersions. *Advances in Colloid and Interface Science* **1996,** *68* (Supplement C), 57-96; (b) Kim, K.; Kim, S.; Ryu, J.; Jeon, J.; Jang, S. G.; Kim, H.; Gweon, D.-G.; Im, W. B.; Han, Y.; Kim, H.; Choi, S. Q., Processable high internal phase Pickering emulsions using depletion attraction. *Nature Communications* **2017,** *8*, 14305.

42.   Arditty, S.; Whitby, C.; Binks, B.; Schmitt, V.; Leal-Calderon, F., Some general features of limited coalescence in solid-stabilized emulsions. *The European Physical Journal E* **2003,** *11* (3), 273-281.

43.   Dridi, W.; Harscoat-Schiavo, C.; Monteil, J.; Faure, C.; Leal-Calderon, F., Monodisperse Oil-in-Water Emulsions Stabilized by Proteins: How To Master the Average Droplet Size and Stability, While Minimizing the Amount of Proteins. *Langmuir* **2018,** *34* (31), 9228-9237.

44.   Oldenburg, S. J.; Averitt, R. D.; Westcott, S. L.; Halas, N. J., Nanoengineering of optical resonances. *Chemical Physics Letters* **1998,** *288* (2), 243-247.

45.   Kim, B. S.; Lee, T. R., The Development of Smart, Multi-Responsive Core@ Shell Composite Nanoparticles. In *Nanoparticles Technology*, InTech: 2015.

46.   Wolinsky, J. B.; Colson, Y. L.; Grinstaff, M. W., Local drug delivery strategies for cancer treatment: gels, nanoparticles, polymeric films, rods, and wafers. *Journal of controlled release* **2012,** *159* (1), 14-26.

47.   Vaklev, N.; Vasileva, N.; Dushkin, C., Synthesis of gold nanoparticles via hydrogen peroxide reduction enhanced by sonication. *Nanoscience and Nanotechnology* **2007,** *7*, 70-73.

48.   Zayats, M.; Baron, R.; Popov, I.; Willner, I., Biocatalytic growth of Au nanoparticles: from mechanistic aspects to biosensors design. *Nano Letters* **2005,** *5* (1), 21-25.

49.   Quintanilla, A.; García-Rodríguez, S.; Domínguez, C. M.; Blasco, S.; Casas, J. A.; Rodriguez, J. J., Supported gold nanoparticle catalysts for wet peroxide oxidation. *Applied Catalysis B: Environmental* **2012,** *111-112*, 81-89.

50.   Hwang, J. H.; Brayman, A. A.; Reidy, M. A.; Matula, T. J.; Kimmey, M. B.; Crum, L. A., Vascular effects induced by combined 1-MHz ultrasound and microbubble contrast agent treatments in vivo. *Ultrasound in medicine & biology* **2005,** *31* (4), 553-564.

51.   Duck, F. A., *Physical properties of tissues: a comprehensive reference book*. Academic press: 2013.

Acknowledgments